Composites Part C: Open Access 9 (2022) 100316

Contents lists available at ScienceDirect

Composites Part C: Open Access

journal homepage: www.elsevier.com/locate/composites-part-c-open-access

Hands-free printed door opener to limit the spread of Coronavirus: Design through topology optimization

Enrico Panettieri, Giulia Bertolino, Marco Montemurro *

Arts et Métiers Institute of Technology, Université de Bordeaux, CNRS, INRA, Bordeaux INP, HESAM Université, I2M UMR 5295, F-33405 Talence, France

ARTICLE INFO

Keywords:
Topology optimization
Additive manufacturing
NURBS Hyper-surfaces
Density-based method
Manufacturing constraints
COVID

ABSTRACT

Recently, the necessity of reducing the probability of spread of viruses has fostered the creativity of engineers to develop tools that would allow actions of every-day life to be executed differently. Moreover, the maturity of the Fused Filament Fabrication (FFF) technology and the associated low costs has allowed creative solutions to be produced and used in real-life applications. A distinctive example is represented by the common action of opening a door. Since hands are a typical vector of contamination for viruses such as Coronavirus, hands-free devices aim at making use of the existing structure and kinematic to complete the same action in a different fashion. Typically, the mechanical and manufacturing requirements of these devices include a suitable stiffness-to-mass ratio, a reduced printing time as well as the minimization of supports which need to be removed in a post-printing phase. To tackle all these requirements a dedicated topology optimization (TO) method can be used since the preliminary design phase. Several design requirements of different nature can be included in the problem formulation: mechanical ones, like mass and stiffness, and manufacturing ones, like drawing direction or minimum member size. In this paper, a feasibility study on a hands-free 3D printed door opener has been carried out by means of the Solid Isotropic Material with Penalization (SIMP) method for TO and its CAD-compatible variant, i.e., the SIMP approach reformulated in the framework of non-uniform rational basis spline hyper-surfaces. The aim of the study is to identify optimal solutions to be adapted to a real-case scenario wherein different loading cases and manufacturing constraints are evaluated. Different optimal solutions are obtained, reconstructed to be compatible with CAD environment and the optimized geometry numerically assessed. Finally, the optimal solutions are also evaluated with respect to indicators such as printing time, total filament mass and mass of the supports required by the printing process.

1. Introduction

Nowadays the development of additive manufacturing technologies allows engineers to develop new design approaches capable of devising more efficient solutions to existing problems. Almost all the industrial sectors are somehow impacted as new design approaches, new tools for numerical analyses and new testing protocols are emerging to harness the potential of this still evolving technology [1–5].

One of the main advantages of the 3D printing lies in the possibility of producing extremely complex geometries [2] otherwise impossible to manufacture with traditional processes such as forging, casting, machining, etc. Moreover, recent developments of both the 3D printing technology and of the associated design tools allow for the same component to tackle different mechanical functions by making use of multiple materials in the printing process [6]. Another aspect, which has drawn the attention of many industrial sectors, is that 3D printing allows to drastically reduce the time between design and manufacturing which, as a consequence, leads to the possibility of improving the final design by successive iterations. For example, in the biomedical sector, this has allowed to facilitate and to ameliorate the production of customized prostheses and implants [5].

These unique advantages make 3D printing the most suitable manufacturing process for those intricate geometries resulting from one of the most advanced structural optimization approaches such as topology optimization (TO) [7]. The goal of TO is to find the best material distribution, over a domain, in order to minimize a given cost function while, at the same time, complying with a set of requirements of different nature, e.g., mechanical, thermal, electrical and including constraints related to the manufacturing process. Today, the most popular numerical methods developed to solve TO problems are density-based TO methods based on the Solid Isotropic Material with Penalization (SIMP) scheme [8–12] and the Level-Set Method (LSM) [13–16]. Among these two methods, the density-based approach coupled with SIMP scheme is

* Corresponding author.
E-mail addresses: marco.montemurro@ensam.eu, marco.montemurro@u-bordeaux.fr (M. Montemurro).

https://doi.org/10.1016/j.jcomc.2022.100316
Received 6 August 2022; Received in revised form 6 October 2022; Accepted 7 October 2022
Available online 18 October 2022

the most used in commercial FE software such as OptiStruct [17] and TOSCA [18]. In density-based TO methods, the pseudo-density, defined in the interval $[0, 1]$, is introduced to penalize the mechanical properties of each element constituting the finite element (FE) model approximating the nominal geometry of the domain to optimize. However, this density-based algorithm is characterized by three main drawbacks. Firstly, due to the FE-based description of the design domain, a smooth CAD-compatible solution can be obtained through a *a-posteriori*, time-consuming reconstruction phase. Secondly, the optimized topology depends upon the mesh quality and size. Thirdly, the structural performances and the satisfaction of the optimization constraints after the reconstruction phase is not ensured.

To overcome these issues, the classic density-based TO method was modified by introducing Non-uniform Rational Basis Splines (NURBS) entities to represent the pseudo-density field. A new TO algorithm, called SANTO (SIMP And NURBS for Topology Optimization) was developed at the I2M laboratory in Bordeaux [19–28].

The recent pandemic of COVID-19 has shown how 3D printing technologies have been able to rapidly adapt and to respond to the need of crucial healthcare supplies, such as, for example, components for respirators, medical glasses, face shields, hands-free door openers, mask adjusters, ventilator splitters, oxygen filter housings, etc. [29–34]. Among these supplies, those for which a very large number of designs was proposed were face shields, respirators, and hands-free devices to limit the diffusion of the virus [29,31–34]. Nevertheless, the works dealing with the design of hands-free door openers [32–34] focus, very often, on aesthetic and manufacturing aspects, without considering an automatic numerical design procedure involving modern generative design software, like TO algorithms.

This work proposes a feasibility study on a hands-free 3D printed door opener via two design approaches involving two different topology optimization schemes: a classical density-based TO method making use of the SIMP interpolation technique, and the NURBS-based SIMP method. The objective is twofold: to identify optimized solutions for the door opener where different loading cases and manufacturing constraints are considered and to evaluate the optimal solutions with respect to indicators related to the 3D printing process such as the printing time, the total filament mass and the quantity of supports necessary to a successful printing.

A focus is put on the influence of different material properties used to characterize the mechanical behavior on the final result as well as the presence of manufacturing constraints defining the minimum size of the topological features in the optimal solutions (which is related to the limits of the FFF 3D printing technology) and the definition of a drawing direction of the topological features which could limit the presence of supports.

The paper is organized as follows. The hands-free door opener study case is described in Section 2. The values of the two sets of material properties used in the TO runs are presented in Section 3. The problem formulation as well as the theoretical background of both the SIMP method and of the SANTO algorithm are briefly recalled in Section 4. In Section 5, the FE models created for the TO runs with the OptiStruct module and the SANTO algorithm are described. The results of the sensitivity analyses carried out on the material properties and the optimization constraints are shown in Section 6. Section 7 highlights the impact of the different optimal topologies on the printing time, the total filament mass and quantity of supports. Finally, Section 8 ends the paper with some conclusions.

2. Presentation of the study case

The study case deals with the optimal design of a door opener device designed to allow a door-handle being used without hands. The door opener device must be adaptable to standard door-handles, as shown in Fig. 1. The same figure also shows the design domain, the hinge axis and the region where the forearm applies the effort required to guide the rotation of the door-handle allowing the door being opened.

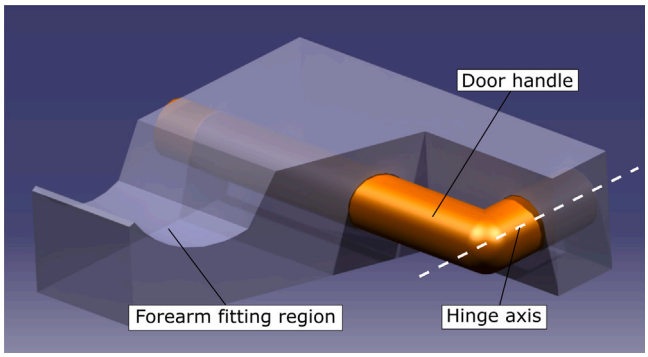

Fig. 1. CAD render of a generic door-handle, of its hinge axis, the design domain and the fitting region where the forearm applies the required efforts.

Table 1
PLA base material properties from specimens printed with a layer thickness equal to 0.2 mm [35,36].

Isotropic PLA					
E_p	[MPa]	2462.0	ν	[-]	0.37
Transversely isotropic PLA					
E_{1p}	[MPa]	2816.0	$\nu_{12} = \nu_{13} = \nu_{23}$	[-]	0.37
$E_{2p} = E_{3p}$	[MPa]	2108.0	$G_{12p} = G_{13p}$	[MPa]	780.4
			G_{23p}	[MPa]	769.3

The relevant dimensions of the design domain are shown in Fig. 2. The geometry of the forearm fitting region has been defined *a priori* to allow the operator to apply at the same time a force to guide the rotation of the hinge axis and a force to push the door. To efficiently guide the hinge into rotation, the device should be stiff enough, while to reduce both the use of material and the manufacturing time, lightweight configurations are sought.

FFF 3D printing allows for a great manufacturing freedom when complex topologies have to be manufactured. Nonetheless, manufacturing aspects related to the quantity of printing supports, to the anisotropy of the resulting material according to the printing direction and to the filling strategies must be taken into account to select solutions that comply with the given requirements.

3. Material properties

The Polylactic acid (PLA) plastic is one of the most used materials within the FFF technology because of its low cost as well as its minimal warping issues. Two sets of PLA base material properties are considered: the first one represents a linear elastic isotropic (LEI) material, while the second one is a linear elastic transversely isotropic (LETI) material. Table 1 reports the values of the PLA base material properties extracted from [35,36]. The SIMP penalization law is usually imposed to the elasticity matrix of isotropic materials. Nonetheless, from a numerical point of view, the same penalization scheme can be also applied to the elasticity matrix of non-isotropic materials. The latter case requires to impose *a priori* the material orientation which, in the case of the FFF printing process, can be related with the position of the object with respect to the building plate.

In this study, the influence of the material elastic symmetry, i.e., LETI and LEI cases, on the optimized topology is investigated. As an example, the coordinate system, whose directions correspond to the typical printing directions, of a generic LETI material is provided in Fig. 3(a).

In 3D printing, several filling strategies are proposed to reduce both the overall weight as well as the printing time. The resulting

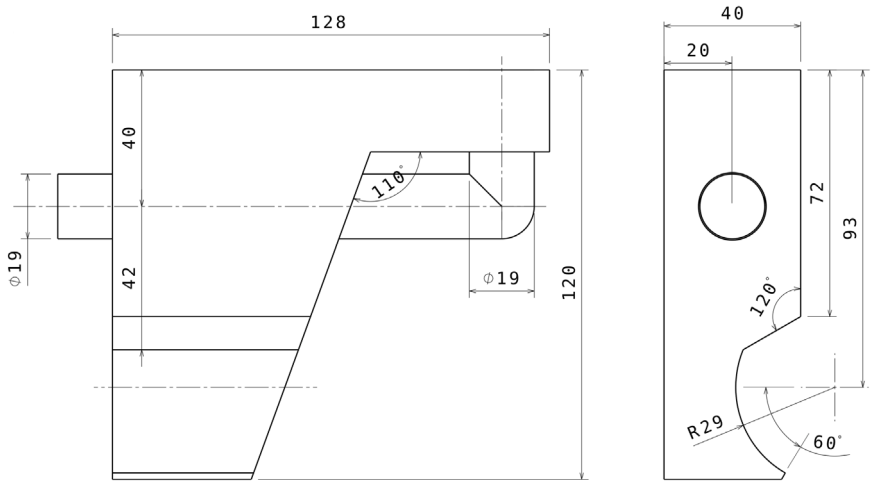

Fig. 2. Geometry of both the door-handle and the design domain.

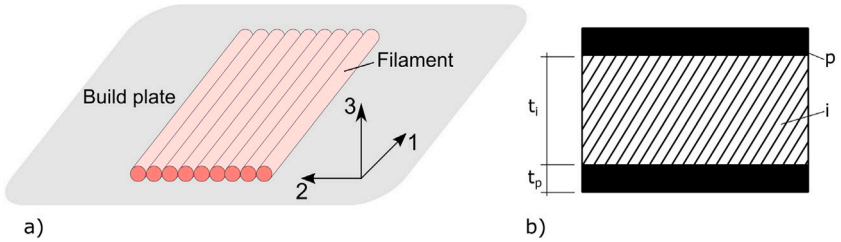

Fig. 3. (a) Example of coordinate system of the LETI material; (b) scheme used to evaluate the knock-down factor when a filling strategy is used.

structure can be seen as a 3D sandwich structure. For this reason, the base material properties are pertinent only when the filling strategy corresponds to 100% fill with a concentric print strategy (concentric filaments following the external shape).

In this study, the base material properties of Table 1 are used to evaluate equivalent material properties through knock-down factors uniformly applied to the engineering constants. The knock-down factor has been estimated by considering a relative density $\alpha = 0.2$.

For the LEI material properties, the scheme used to compute the knock-down factor is represented in Fig. 3(b). The equivalent Young's modulus, E^*, of the assumed elementary volume shown in Fig. 3(b) is computed by means of the rule of mixtures. The Young's modulus of the infill region (label *i* in Fig. 3(b)) is evaluated through the Gibson and Ashby formula [37] as follows:

$$\frac{E_i}{E_p} = \alpha^2, \tag{1}$$

where α is the relative density of the infill region and E_p is the Young's modulus of the base material. In the following of this section, subscript *p* is used to refer to quantities (e.g., material properties) related to the base material.

By applying the rule of mixtures, the value of E^* is obtained as follows:

$$E^* = \frac{2t_p + \alpha^3 t_i}{2t_p + \alpha t_i} E_p. \tag{2}$$

Even though the approach is simplistic, Eq. (2) allows for a conservative value of E^* being estimated as a function of the geometrical parameters t_p and t_i, which depend on the resulting topology. Fig. 4 shows the curves of E^* as a function of t_i and t_p. For the purposes of this study, a conservative value of E^* equal to 1410 MPa has been adopted. This value corresponds to the set of geometrical parameters t_i and t_p equal to 8 mm and 1 mm, respectively. The value of t_i represents an overestimation of that used as minimal member thickness within the TO.

Table 2
Equivalent material properties used in the TO simulations.

Equivalent isotropic PLA (ELEI material)					
E^*	[MPa]	1410	ν	[-]	0.37
Equivalent transversely isotropic PLA (ELETI material)					
E_1^*	[MPa]	1614.0	$\nu_{12} = \nu_{13} = \nu_{23}$	[-]	0.37
$E_2^* = E_3^*$	[MPa]	1208.0	$G_{12}^* = G_{13}^*$	[MPa]	447.4
			G_{23}^*	[MPa]	441.1

For the LETI material properties, the knock-down factor used to reduce the elastic properties (only the Poisson's ratio is kept unchanged) of Table 1 has been computed by using the ratio $\frac{E^*}{E_p}$ of Eq. (2).

The equivalent properties for the linear elastic isotropic base material and for the linear elastic transversely isotropic base material, indicated as ELEI and ELETI materials, respectively, used in the optimization calculations are reported in Table 2. The shear moduli of the ELETI material of Table 2 have been computed by scaling the corresponding value of the base material of Table 1 by the ratio $\frac{E^*}{E_p}$.

4. Problem formulation: theoretical framework and numerical strategy

The literature survey on the numerical methods developed to solve TO problems shows that two methods are widely used in the scientific community: density-based TO algorithms, often based on the SIMP approach [8–12] and the Level-Set Method (LSM) [13–16]. Even though the LSM shows some advantages compared to the SIMP method, in the context of this work, only the fundamentals of density-based TO algorithm based on the SIMP approach are presented as well as those of the NURBS-based SIMP method (and of the related algorithm called SANTO) developed at the I2M laboratory in Bordeaux [19–28]. A detailed description of the LSM for TO is available in [13–16].

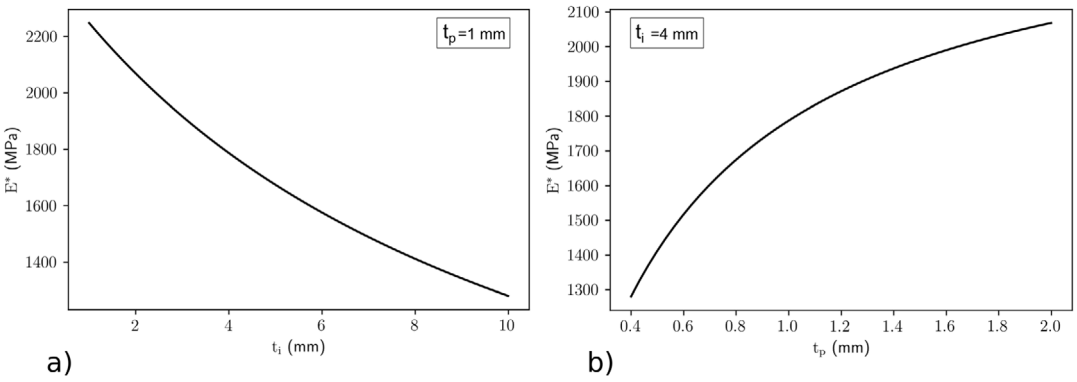

Fig. 4. (a) Equivalent Young's modulus E^* vs. t_i with $t_p = 1$ mm; (b) Equivalent Young's modulus E^* vs. t_p with $t_i = 4$ mm (curves obtained for $\alpha = 0.2$).

4.1. The classic density-based method for topology optimization

The SIMP approach turns the problem of finding an optimal topology into the one of searching for a suitable material distribution in a prescribed domain to minimize a given objective function while satisfying a set of requirements. The goal is to find the optimal distribution of a fictitious homogeneous material by introducing a pseudo-density field variable, $\rho(\mathbf{x}) \in [0,1]$, which penalizes the stiffness tensor of the elements of a given mesh. The value $\rho(\mathbf{x}) = 0$ identifies the void phase, while $\rho(\mathbf{x}) = 1$ represents the solid phase.

Let us consider a domain, $\Omega \subset \mathbb{R}^3$, in the Euclidean 3D space, where a Cartesian orthogonal frame $O(x_1; x_2; x_3)$ is defined. The values of the stiffness tensor, $E_{ijkl}(\rho(\mathbf{x}))$, defined over the domain Ω, are influenced by the pseudo-density field variable, as follows:

$$E_{ijkl}(\rho(\mathbf{x})) = \rho^p(\mathbf{x})\, E^0_{ijkl}, \qquad i,j,k,l = 1,2,3, \tag{3}$$

where $\mathbf{x}$ is the vector collecting the Cartesian coordinates of the generic point of the continuum, whilst E^0_{ijkl} is the stiffness tensor of the bulk material and $p > 1$ is a suitable parameter used to penalize the solution for intermediate values of $\rho(\mathbf{x})$ (typically $p = 3$) [9].

When considering the FE formulation of a static equilibrium problem, under the hypothesis that boundary conditions (BCs) of the Dirichlet type are zero, $\mathbf{d}$ denotes the vector of generalized displacements, i.e., the unknown degrees of freedom (DOFs) and $\mathbf{f}$ is the vector of external nodal forces. The relation between these two quantities can be written as follows:

$$\mathbf{K}\mathbf{d} = \mathbf{f}, \tag{4}$$

where $\mathbf{K}$ represents the global stiffness matrix of the structure. The matrix $\mathbf{K}$ can be expressed as:

$$\mathbf{K} := \sum_{e=1}^{N_e} \rho_e^p \mathbf{L}_e^T \mathbf{K}_e^0 \mathbf{L}_e = \sum_{e=1}^{N_e} \mathbf{L}_e^T \mathbf{K}_e \mathbf{L}_e, \tag{5}$$

where ρ_e is the pseudo-density computed at the centroid of each element, while N_e is the total number of elements of the model. The matrices $\mathbf{K}_e^0$ and $\mathbf{K}_e$ are the pristine and penalized stiffness matrices of element e, respectively, computed with respect to the global coordinate system frame of the FE model. The element connectivity matrix $\mathbf{L}_e$ relates the nodal displacements vector, $\mathbf{d}$, with the vector of nodal displacements of element e, $\mathbf{d}_e$, as follows:

$$\mathbf{d}_e = \mathbf{L}_e \mathbf{d}. \tag{6}$$

With this notation, as discussed in [26], under homogeneous BCs of the Dirichlet type, the compliance of the structure, C, is equal to the work of internal forces and can be computed as:

$$C := \mathbf{d}^T \mathbf{K}\mathbf{d}. \tag{7}$$

Thus, the optimization problem of the minimization of the compliance of a structure subject to a constraint on the volume can be formulated as follows:

$$\min_{\rho_e} C(\rho_e), \qquad \text{subject to :} \quad \begin{cases} \mathbf{K}\mathbf{d} = \mathbf{f}, \\ \dfrac{V(\rho_e)}{V_{\text{ref}}} = \dfrac{\sum_{e=1}^{N_e} \rho_e V_e}{V_{\text{ref}}} \le \gamma, \\ \rho_{\min} \le \rho_e \le 1, \quad e = 1, \dots, N_e, \end{cases} \tag{8}$$

where V_{ref} is the reference volume, $V_e(\mathbf{x})$ is the volume of the generic element of the mesh, γ is the given volume fraction and $\rho_{\min}$ is the lower boundary imposed to the density field to prevent singular values in the stiffness matrix of the elements during the optimization process. Therefore, the design variables of the SIMP method are pseudo-density values evaluated at the centroids of the elements. Consequently the total number of variables is equal to N_e.

The simplicity of the SIMP approach as well as its straightforward implementation within commercial FE codes is nonetheless prone to a well-known numerical issue related to the lack of mutual dependency among the values of the pseudo-density defined at each element centroid. This issue is usually known as checker-board effect. To overcome this issue, a distance-based filter technique [10] and the use of higher order finite elements are usually employed [38].

4.2. The NURBS-based SIMP method

As widely discussed in [21–28,39], the main difference between the classic SIMP approach and the NURBS-based SIMP method is that, in the latter approach, the pseudo-density field, $\rho(\mathbf{x})$ is described by means of a NURBS entity. Particularly, for a problem of dimensions D, a NURBS hyper-surface of dimension $D+1$ is required to describe the topology. Thus, for a 3D problem, a 4D NURBS entity is needed: the first three coordinates are used to define the 3D design domain, whilst the last one is the scalar pseudo-density field that reads

$$\rho(\zeta_1, \zeta_2, \zeta_3) := \sum_{i_1=0}^{n_1} \sum_{i_2=0}^{n_2} \sum_{i_3=0}^{n_3} R_{i_1,i_2,i_3}(\zeta_1, \zeta_2, \zeta_3) \rho_{i_1,i_2,i_3}, \tag{9}$$

where $n_{\text{CP}} := \prod_{i=1}^{3}(n_i + 1)$ is the total number of control points, ρ_{i_1,i_2,i_3} is the pseudo-density at the generic control point, while $\rho(\zeta_1, \zeta_2, \zeta_3)$ is the pseudo-density field depending on the dimensionless parameters ζ_j, which are related to the Cartesian coordinates as follows:

$$\zeta_j := \frac{x_j}{a_j}, \quad j = 1,2,3. \tag{10}$$

The term $R_{i_1,i_2,i_3}(\zeta_1, \zeta_2, \zeta_3)$ in Eq. (9) represents the NURBS rational basis functions which reads:

$$R_{i_1,i_2,i_3}(\zeta_1, \zeta_2, \zeta_3) := \frac{\omega_{i_1,i_2,i_3} \prod_{k=1}^{3} N_{i_k,p_k}(\zeta_k)}{\sum_{j_1=0}^{n_1} \sum_{j_2=0}^{n_2} \sum_{j_3=0}^{n_3} \left[\omega_{j_1,j_2,j_3} \prod_{k=1}^{3} N_{j_k,p_k}(\zeta_k) \right]}, \tag{11}$$

where $N_{i_k,p_k}(\zeta_k)$ are the Bernstein's polynomials of degree p_k [40] and ω_{j_1,j_2,j_3} are suitable weights that influence the way the NURBS entity is attracted towards a given control point.

In the context of the NURBS-based SIMP method, the design variables are the pseudo-density values at the control points and the associated weights. They are included in the design variable vectors $\boldsymbol{\xi}_1$ and $\boldsymbol{\xi}_2$, which are defined as:

$$\boldsymbol{\xi}_1^{\mathrm{T}} := \left(\rho_{000}, \dots, \rho_{n_1 n_2 n_3}\right), \ \boldsymbol{\xi}_2^{\mathrm{T}} := \left(\omega_{000}, \dots, \omega_{n_1 n_2 n_3}\right), \ \boldsymbol{\xi}_1, \boldsymbol{\xi}_2 \in \mathbb{R}^{n_{\mathrm{CP}}}, \quad (12)$$

accordingly, the number of design variables is, at most, $n_{\mathrm{var}} = 2n_{\mathrm{CP}}$. The other parameters, i.e., number of control points, basis functions degrees, components of the knot vector along each parametric direction, are set *a priori* by the user and do not change during the optimization process [19,20]. Subsequently, the pseudo-density field described through the NURBS entity is used to penalize the global stiffness matrix of the structure according to Eq. (5).

In this background, the problem of minimizing the compliance of the continuum subject to a constraint on the volume reads:

$$\min_{\boldsymbol{\xi}_1,\boldsymbol{\xi}_2} \ \frac{C(\boldsymbol{\xi}_1,\boldsymbol{\xi}_2)}{C_{\mathrm{ref}}}, \ \text{subject to} : \begin{cases} \mathbf{Kd} = \mathbf{f}, \\ \dfrac{V}{V_{\mathrm{ref}}} \le \gamma, \\ \boldsymbol{\xi}_{1\tau} \in [\rho_{\min}, \rho_{\max}], \quad \boldsymbol{\xi}_{2\tau} \in [\omega_{\min}, \omega_{\max}], \\ \tau = 1, \dots, n_{\mathrm{CP}}. \end{cases} \quad (13)$$

The choice of representing the pseudo-density field through a NURBS entity presents several advantages with respect to the classic density-based methods: (1) the total number of design variables is not related to the number of elements constituting the mesh, (2) since a pure geometric CAD-compatible entity is used as a topological descriptor, the optimized solution is not affected by the quality of the mesh of the FE model, (3) the presence of the local support property (see [40]) allows for an implicit filtering effect which prevent numerical artifacts (e.g., checker-board effect) to appear. Finally, a further advantage of the NURBS-based SIMP method is in the handling of the geometric constraints imposed on the topological variable. Particularly, since the pseudo-density field describing the topology of the continuum is described by means of a NURBS hyper-surface, it is possible to properly set the integer parameters (i.e., number of control points and basis functions degree p_j along each parametric direction) governing its shape to automatically satisfy the minimum length scale requirement, without introducing an explicit optimization constraint in the problem formulation [21]. For a detailed description of the NURBS-based SIMP method, the reader is addressed to [21–28].

The NURBS-based SIMP approach has been integrated into the SANTO algorithm, which is coupled with the ANSYS FE software to evaluate the structural responses included in the problem formulation (and the related gradients). An overview of the workflow of the SANTO algorithm is shown in Fig. 5.

4.3. Formulation of the optimization problem

The design problem is usually formulated as a constrained nonlinear programming problem (CNLPP) where an objective function is minimized while meeting a set of optimization constraints. The optimization constraints can be of different nature: mechanical, geometrical and related to manufacturability requirements.

In this study, when the classic density-based TO method is used, the CNLPP is stated as follows:

$$\min_{\rho_e} \ \frac{V(\rho_e)}{V_{\mathrm{ref}}}, \ \text{subject to} : \begin{cases} \mathbf{Kd} = \mathbf{f}, \\ g_d(\rho_e) := |\delta_C| - \delta_{\max} \le 0, \\ g_r(\rho_e) := |\theta_C| - \theta_{\max} \le 0, \\ g_m(\rho_e) \le 0, \\ \rho_e \in [\rho_{\min}, 1], \quad e = 1, \dots, N_e. \end{cases} \quad (14)$$

In Eq. (14), V_{ref} is the volume of the design region for the initial solution, $V(\rho_e)$ is the effective volume of the design region domain depending on the scalar field of the pseudo-density $\rho(\boldsymbol{x})$, ρ_e is the pseudo-density value at the generic element centroid belonging to the design region domain (constituted of N_e elements), $\rho_{\min}$ is the lower bound value imposed to the pseudo-density variable ρ_e. The optimization constraints $g_d(\rho_e)$ and $g_r(\rho_e)$ represents the mechanical constraints on the displacement (δ_C) and the rotation (θ_C) at point C, respectively, as shown in Fig. 6. The maximum values of the displacement at point C, computed with respect to the Z-axis of the global coordinate system, and the rotation at point C, computed with respect to the X-axis of the global coordinate system, are $\delta_{\max} = 1$ mm and $\theta_{\max} = 5°$, respectively. Eventually, additional manufacturing constraints, generically highlighted in Eq. (14) as $g_m(\rho_e)$, are imposed, as detailed in Section 6.

Finally, when considering the NURBS-based SIMP method, the problem formulation reads:

$$\min_{\boldsymbol{\xi}_1,\boldsymbol{\xi}_2} \ \frac{V(\boldsymbol{\xi}_1,\boldsymbol{\xi}_2)}{V_{\mathrm{ref}}}, \ \text{subject to} : \begin{cases} \mathbf{Kd} = \mathbf{f}, \\ g_d(\boldsymbol{\xi}_1,\boldsymbol{\xi}_2) := |\delta_C| - \delta_{\max} \le 0, \\ g_r(\boldsymbol{\xi}_1,\boldsymbol{\xi}_2) := |\theta_C| - \theta_{\max} \le 0, \\ g_m(\boldsymbol{\xi}_1,\boldsymbol{\xi}_2) \le 0, \\ \boldsymbol{\xi}_{1\tau} \in [\rho_{\min}, \rho_{\max}], \quad \boldsymbol{\xi}_{2\tau} \in [\omega_{\min}, \omega_{\max}], \\ \tau = 1, \dots, n_{\mathrm{CP}}. \end{cases} \quad (15)$$

The gradient of the structural responses, like volume, generalized displacements, etc. are reported in [10] in the case of the classic density-based TO method and in [22,41] for the NURBS-based SIMP method.

5. Description of the finite element models

5.1. Finite element model coupled with the SIMP method: the OptiStruct module

The CAD geometry of the initial volume of the door opener device, shown in Fig. 1, has been imported into Hypermesh and partitioned to identify design and non-design regions, as shown in Fig. 6(a), in red and blue, respectively. Additional partitions have been created to force the generation of elements with limited distortion. Linear hexahedral elements (HEX8), with eight nodes and three degrees of freedom (DOFs) per node, have been chosen and a total number of approximately 90000 elements (corresponding to an average mesh size of 1.5 mm), has been found to be a good compromise between computational costs and accuracy of results. The mesh used for the TO is shown in Fig. 6(b).

To impose boundary conditions and to apply external loads, rigid links have been created between three reference nodes, i.e., nodes A, B and C, and those nodes belonging to adjacent surfaces as shown in Fig. 6(c). The suppressed DOFs at nodes A and B, with respect to the global coordinate system, are those which allow to reproduce the kinematics of the device of Fig. 2. The relevant boundary conditions

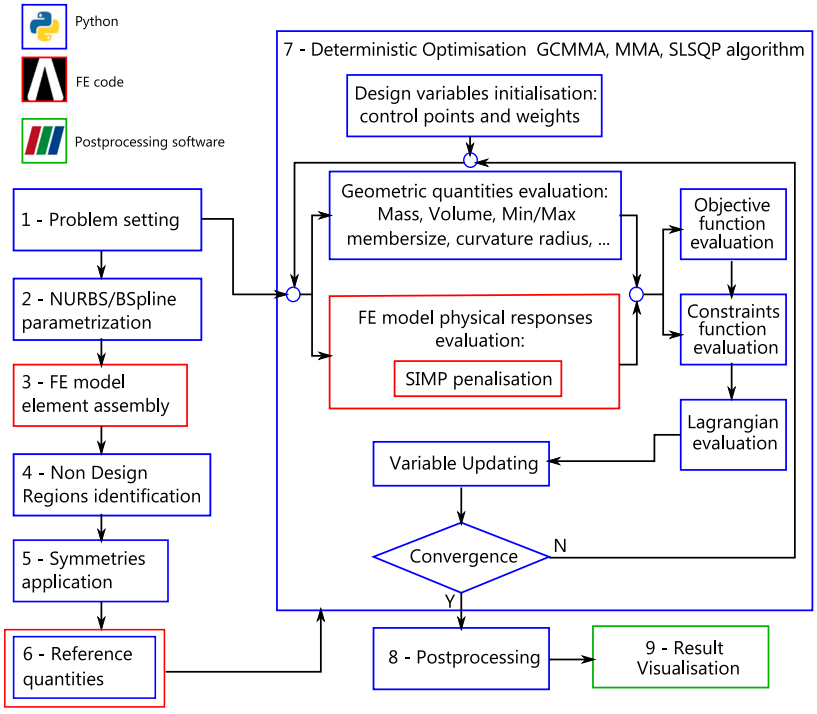

Fig. 5. Flowchart of the SANTO algorithm.

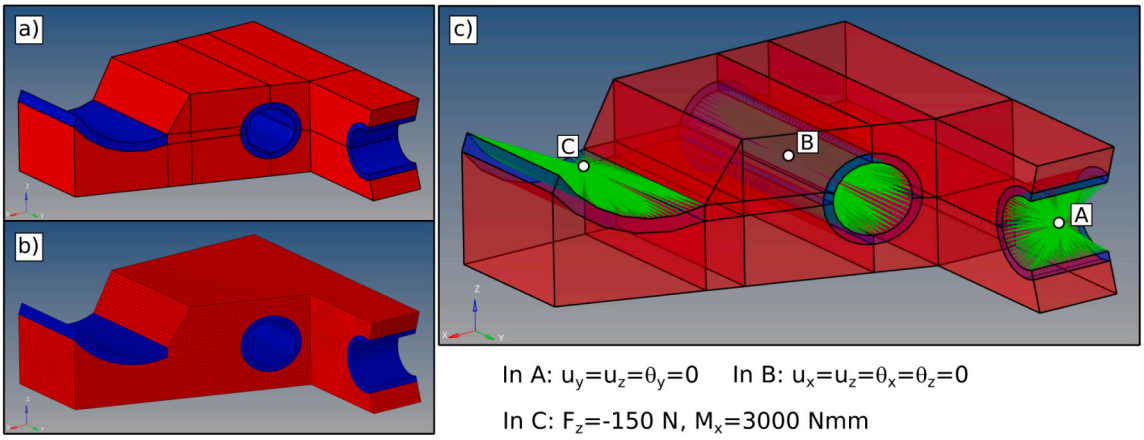

Fig. 6. (a) Partitioned geometry, (b) mesh and (c) boundary conditions of the FE model used within OptiStruct environment. Red and blue regions correspond to design and non-design regions, respectively. (For interpretation of the references to color in this figure legend, the reader is referred to the web version of this article.)

applied to nodes A and B are reported in Fig. 6. Point C represents the node where the resultant of the distribution of pressure on the functional surface of the door opener is applied. As external loads, the following components of the resultant force and moment have been considered for the TO: $\overline{F}_z = -150\ N$ and $\overline{M}_x = 3000$ Nmm (estimated as the torque resulting by applying $\overline{F}_z$ at the border of the non-design region at a distance of approximately 20 mm). A static linear analysis is carried out to determine the structural responses involved in the CNLPP of Eq. (14).

5.2. Finite element model coupled with the NURBS-based SIMP method: the ANSYS environment

The FE model of the overall design volume of the door opener device interfaced with the NURBS-based SIMP method, available in SANTO, is shown in Fig. 7. This model is generated through an ad-hoc script within the ANSYS environment by exploiting the Ansys Parametric Design Language (APDL). In particular, APDL has been used to generate the partitions needed to obtain a structured mesh of approximately 80000 SOLID185 elements (an 8-node solid element characterized by three DOFs per node). The average mesh size used is approximately 2 mm since one of the advantage of using the NURBS-based SIMP method is that the TO solution is remarkably less sensitive to the mesh size. Multi-point constraints elements (MPC184 with two nodes and six DOFs per node) with a rigid beam behavior have been created at nodes A, B, C to apply BCs to the nodes belonging to the relevant surfaces of non-design regions. The same set of BCs of the FE model generated in the OptiStruct environment, as reported in Fig. 6, has been used, by adapting the applied forces and moments to the global frame used in ANSYS environment.

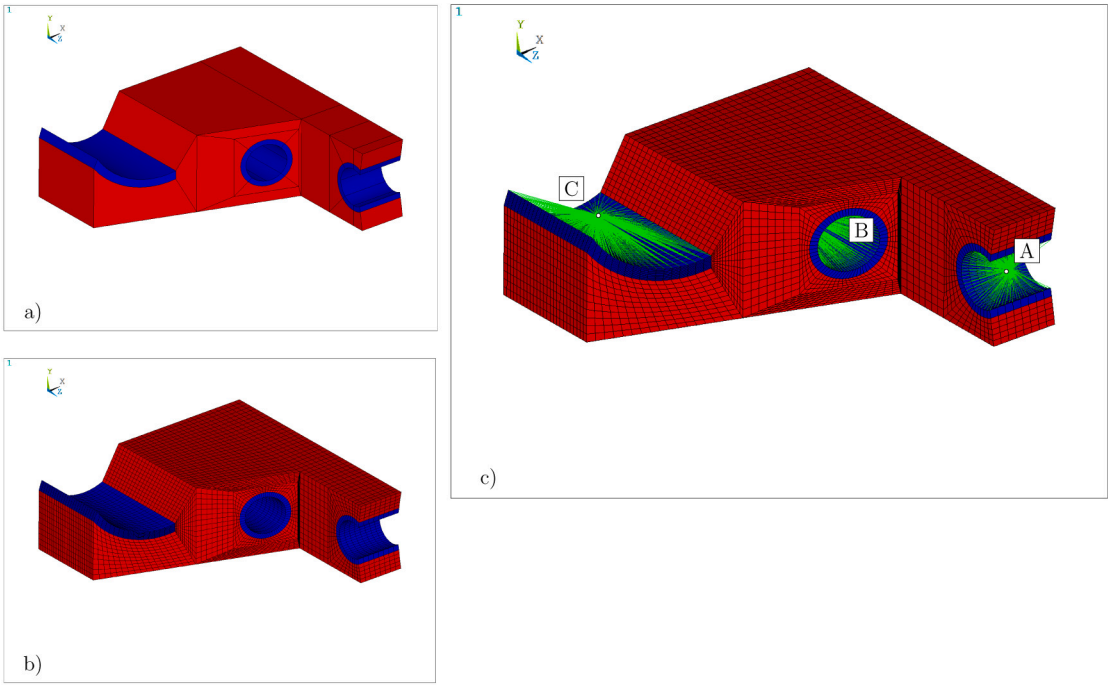

Fig. 7. (a) Model geometry, (b) mesh and (c) boundary conditions of the FE model used for the NURBS-based SIMP method. Red and blue regions correspond to design and non-design regions, respectively. (For interpretation of the references to color in this figure legend, the reader is referred to the web version of this article.)

6. Topology optimization: sensitivity to manufacturing constraints

To address light-weight and stiff solutions that minimize the presence of support material during the manufacturing, a sensitivity analysis of the optimized topology to the manufacturing constraints of different nature has been carried out. Moreover, solutions with both equivalent isotropic and equivalent transversely isotropic materials have been evaluated for each manufacturing constraint.

The manufacturing constraints that have been considered are listed as follows:

- The minimum member size, $d_{\min}$, which represents the minimum admissible size of the structural solution. In density-based TO algorithm based on the SIMP approach, the value of $d_{\min}$ is related to the average mesh size, e_{avg}. In the OptiStruct environment, the value of $d_{\min}$ must be chosen to be at least three times the value of e_{avg}. Moreover, this requirement is formulated as an explicit optimization constraint in the problem formulation. Conversely, when using the NURBS-based SIMP method, this requirement is handled without introducing an explicit optimization constraint in the problem formulation. Indeed, as discussed in [21], the minimum length scale requirement can be handled by properly setting the number of control points and the degrees of the Bernstein's polynomials.
- The drawing direction, which represents the direction along which the TO algorithm is allowed to locally suppress material. This constraint, in the context of the FFF technology, can be linked to the printing direction which is normal to the building plate (direction 3 of Fig. 3).

The effect of the drawing direction manufacturing constraint has been evaluated by considering two perpendicular directions (corresponding to two of the axes of the global coordinate system of the FE model), as highlighted in Fig. 8. The Y-drawing and the Z-drawing directions define a direction used by the solver to seek for optimal material distribution within the initial domain. In the context of the FFF technology, the constraint on the drawing direction can be used to seek for those optimal solutions which minimize the quantity of supports during the manufacturing.

Table 3
Overview of the TO analyses (the value of $d_{min} = 4.5$ mm has been kept constant within all TO simulations).

Manufacturing constraint		Values	
Minimum member size, d_{min}	[mm]	4.5	10
Drawing direction	[-]	Y-direction	Z-direction

Possibly, since in the FFF technology the manufacturing direction influences the resulting material properties, when TO is performed by considering the ELETI material properties (whose material properties have been defined in Table 2), material orientation is modified accordingly by defining *ad-hoc* material coordinate systems as reported in Fig. 8. For those TO runs including the optimization constraint on the minimum member size with the ELETI material properties, the material orientation is assumed equal to that used for the optimization constraint on the Y drawing direction.

An overview of the values used for the sensitivity analyses on the manufacturing constraints is shown in Table 3. The comparison of the results obtained with the density-based TO algorithm (OptiStruct) and those obtained with the NURBS-based SIMP method (SANTO algorithm) is solely performed for the formulations of the optimization problems where the constraint on the minimum member size, d_{min}, is equal to 4.5 mm. It is noteworthy that to satisfy the minimum length scale requirement without introducing an explicit optimization constraint in the problem formulation, according to the methodology discussed in [21], a B-spline hyper-surface with a number of control points and degrees of blending functions equal to $n_{\text{CP}} = 36\times36\times12$ and $p_j = 3$ $(j = 1, 2, 3)$, respectively, has been used.

For each optimized solution, a reconstruction of the boundary has been performed via the OSSmooth topology reconstruction module of the Hypermesh suite. This tool allows regenerating an optimized solution by choosing a pseudo-density threshold value. The choice of the threshold value is to some extent user-dependent since its choice affects the resulting reconstructed geometry as well as the respect of

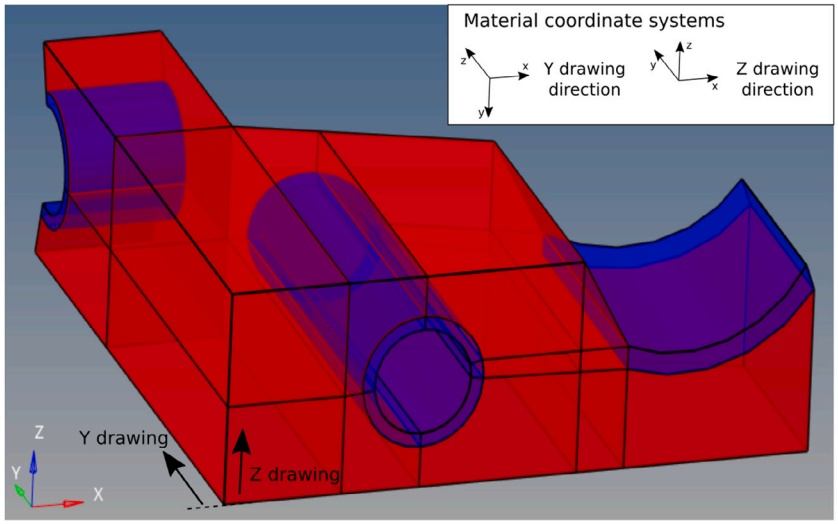

Fig. 8. Drawing directions and material coordinate systems used to assign the ELETI material properties.

Table 4
Overview of the mechanical quantities of the reconstructed TO solutions obtained with the OptiStruct module.

	Mat. props [−]	Constr. value [−]	Run ID [−]	Volume fraction [−]	Density threshold [−]	δ_C [mm]	θ_C [°]
d_{min}	ELEI	4.5 mm	1	0.1204	0.1	−0.96	1.05
		10 mm	2	0.1795	0.1	−0.74	0.77
	ELETI	4.5 mm	3	0.1433	0.1	−0.95	0.83
		10 mm	4	0.1930	0.1	−0.76	0.84
Drawing Dir.	ELEI	Y	5	0.3763	0.2	−0.64	0.19
		Z	6	0.1474	0.2	−0.92	1.34
	ELETI	Y	7	0.3882	0.2	−0.70	0.21
		Z	8	0.1603	0.2	−0.95	1.37

Table 5
Overview of the mechanical quantities of the reconstructed TO solutions obtained with the SANTO algorithm.

	Mat. props [−]	Constr. value [−]	Run ID [−]	Volume fraction [−]	Density threshold [−]	δ_C [mm]	θ_C [°]
d_{min}	ELEI	4.5 mm	9	0.4784	0.03	−0.39	0.12
	ELETI	4.5 mm	10	0.4679	0.04	−0.45	0.09

the imposed manufacturing constraints. For this reason, the value of the pseudo-density threshold, complying with the imposed optimization constraints, is sought through manual iterations. Differently, with the SANTO algorithm, the value of the pseudo-density threshold complying with the imposed constraints is automatically computed in order to satisfy all the optimization constraints.

6.1. TO solutions: mechanical response

For the analyses carried out with the OptiStruct module, suitable threshold values are selected by iterations (to comply with the imposed optimization constraints on the minimum member size) and the corresponding TO solutions are reconstructed and their mechanical behavior assessed with a linear static FE analysis. Each optimal solution is then assessed by applying the same set of boundary conditions, material properties and external loads of the initial FE model to evaluate the displacement, U_Z, and rotation, θ_x, at the loading point (point C of Fig. 6) as well as the value of the volume fraction after reconstruction. The values of volume fractions are computed as the ratio between the volume of the design region, at the given threshold value, at the end of the optimization process and the initial volume of the design region.

Tables 4 and 5 present the results of the sensitivity analyses on the manufacturing constraints evaluated with the two material systems (ELEI and ELETI material) by means of the OptiStruct module and of the SANTO algorithm, respectively.

Regarding the optimized solutions obtained with the OptiStruct module listed in Table 4, the results show that, for all the TO run, the reconstructed FE models respect the optimization constraints on both the maximum displacement, δ_{max}, and the maximum rotation, θ_{max} at point C. As far as the results obtained with the SANTO algorithm are concerned, the optimized topologies after the CAD reassembly phase [42] always satisfy the optimization constraints. However, since the ratio of the number of control points used to describe the NURBS hyper-surface to the number of elements of the FE model is approximately 0.19, the obtained topologies are characterized by a higher volume fraction and, thus, are stiffer than those obtained with the OptiStruct module. Moreover, it is noteworthy the solutions listed in Table 5 have been obtained with a number of design variables equal to about two tenth of those used in the OptiStruct module.

Fig. 9 shows a graphical comparison of the results of Tables 4 and 5. As the comparison of the bar plots highlights, the impact of the material properties (ELEI or ELETI) on the optimal solutions is negligible on both the final volume fraction and the mechanical quantities U_Z and θ_{max}. As far as the considered sensitivity analysis is concerned, the feasible optimized topology characterized by the smaller volume fraction corresponds to Run ID 1 of Table 4.

Figs. 10 and 11 show the optimal topologies of the ten TO runs of Tables 4 and 5. It stands out that the modification of the material properties has, as observed on the structural results, a small influence on the final topology since only local topology modifications occur. This is mainly due to the fact that small differences exist between the values of the ELEI material properties and those of the ELETI material. Nonetheless, the TO runs carried out with the ELETI material properties are those closer to the results obtained with more detailed FE models, as discussed in Section 6.2.

All the reconstructed FE models have been assessed to check for the respect of the manufacturing constraints imposed to the optimization problems. Both the constraints on the minimum member size and on the drawing direction are generally respected within the design domain. In particular, for the TO runs carried out with the OptiStruct module, by adjusting the pseudo-density threshold value it has been possible to generate optimal solutions complying with the constraints imposed on the minimum member size (run IDs 1, 2, 3, and 4).

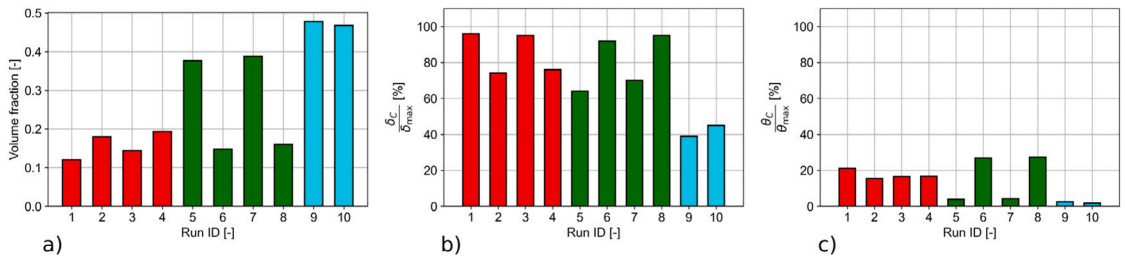

Fig. 9. Overview of the results of Tables 4 and 5: (a) volume fraction, (b) δ_C in percentage with respect to δ_{max} and (c) θ_C in percentage with respect to θ_{max}. Bars in red and green correspond to the results obtained with the OptiStruct module including the d_{min} constraint and the drawing direction constraint, respectively. The cyan bars correspond to the results obtained with the SANTO algorithm. (For interpretation of the references to color in this figure legend, the reader is referred to the web version of this article.)

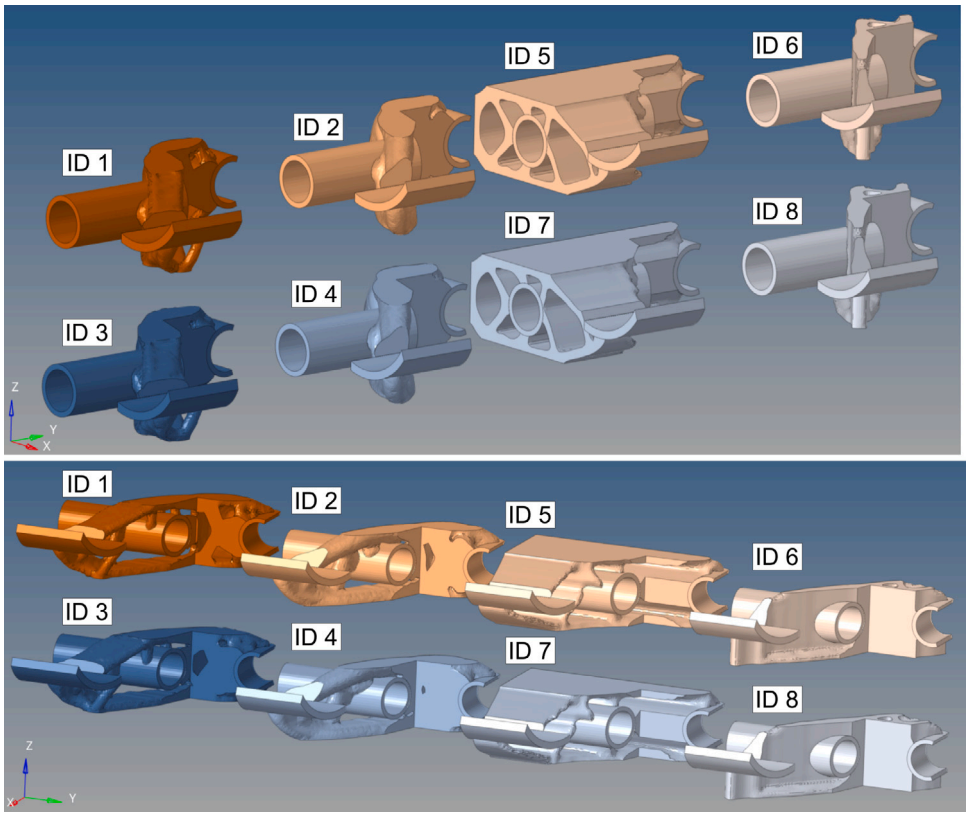

Fig. 10. Optimal topologies of the TO runs of Table 4 obtained with the OptiStruct module.

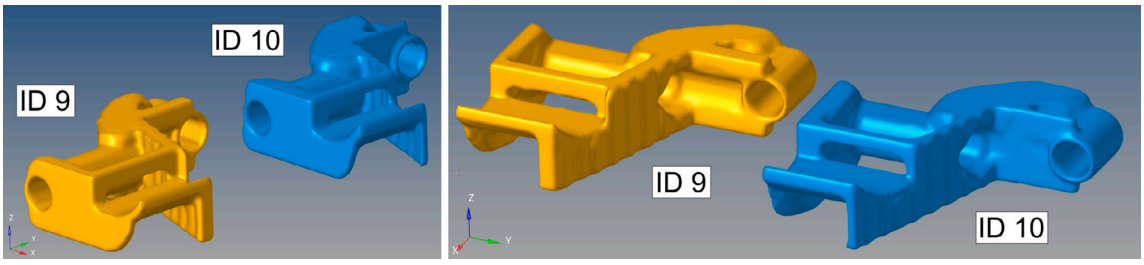

Fig. 11. Optimal topologies of the TO runs of Table 5 obtained with the SANTO algorithm.

Finally, the comparison between the optimal solutions obtained with the OptiStruct module and those of the SANTO algorithm points out the remarkable differences of the optimal topologies obtained at the end of the optimization iterations, which constitutes a sort of "numerical proof" of the non-convexity of the CNLPP considered in this study.

6.2. TO solutions: assessment via shell-solid FE modeling

The assumption used to obtain the equivalent material properties of Table 1 have allowed TO runs to be carried out. These properties reproduce the presence of both the external skin and the infill region as shown in Fig. 3(b) by means of an analytical relationship [37]. Yet,

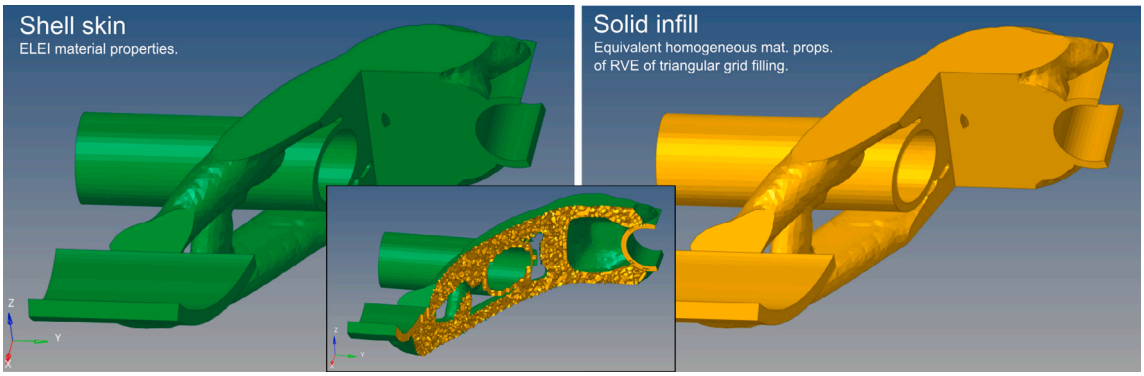

Fig. 12. Modeling strategy adopted to assess the mechanical behavior of the TO solutions obtained with the ELETI material.

this assumptions considers that the thicknesses t_i and t_p of Fig. 3(b), used to compute the equivalent material properties, are kept constant. This hypothesis is seldom applicable in TO since the thickness of the topological features is, unless constrained, not constant. For this reason, additional numerical analyses have been carried out on the optimal solutions obtained with the ELETI material properties to evaluate the error on δ_C and θ_C involved in the CNLPP formulation and used to compare the mechanical responses of the different optimal solutions.

Fig. 12 illustrates the numerical strategy developed to obtain the mechanical response of the door opener when both the external continuous skin and the internal infill, which is a triangular grid infill with a relative density of 20% as shown in Fig. 13, are included in the simulations.

The external element faces surrounding the topology to simulate have been converted into shell elements for which a thickness of 1 mm characterized with the isotropic bulk PLA material properties of Table 1 have been used.

To inject the relevant material properties of the selected infill geometry within the numerical analyses, a numerical linear homogenization [43,44] is previously performed on the representative volume element (RVE) of Fig. 13. The FE model of the RVE has been created within the Abaqus FE commercial software and Periodic Boundary Conditions (PBCs) have been applied via a dedicated Python script. The FE mode of the RVE is composed of $N_{e,\mathrm{RVE}} = 160000$ C3D8 solid elements, for which a sensitivity analysis on the mesh size was performed but not reported in the present work for sake of brevity. Moreover, for the computation of the equivalent elastic properties, the values of the material properties assigned to the RVE of Fig. 13 were those of the PLA bulk material reported in Table 1. Table 6 shows the equivalent material properties of the selected RVE.

The infill equivalent material properties have been assigned to the solid infill, as shown in Fig. 12, via suitable material orientation coordinate systems which correspond to those used in the numerical simulations on the reconstructed optimal solutions obtained with the ELETI material properties.

The comparison between the mechanical response, in terms of δ_C and θ_C, of the simulations carried out with the ELETI material and those performed with the shell-solid strategy is reported in Table 7 and, graphically, in Fig. 14. It is noteworthy that the run ID 3 is that for which the relative error on δ_C is smaller. This result is probably due to the fact that with the constraint on $\mathrm{d_{min}} = 4.5$ mm, the resulting structure is locally characterized by values of $t_i = 4$ mm and $t_p = 1$ mm of Fig. 3(b), which are close to those used to compute the ELETI properties of Table 2. Conversely, greater errors are obtained when bulkier solutions are addressed, e.g., run ID 4, 8 and 10.

7. 3D printing indicators: printing time and use of filament

The TO solutions obtained with the ELETI material properties have been used to evaluate the impact of the manufacturing constraints

Table 6
Equivalent material properties of the RVE of the triangular grid filling strategy with a relative density of 20 %.

E_1 [MPa]	196.0	ν_{12} [-]	0.255	G_{12} [MPa]	51.4
E_2 [MPa]	189.1	ν_{23} [-]	0.139	G_{23} [MPa]	96.0
E_3 [MPa]	501.6	ν_{31} [-]	0.37	G_{31} [MPa]	93.1

Table 7
Overview of the mechanical response of the TO solutions modeled via the shell-solid infill approach. Only the TO solutions characterized by the ELETI materials are considered.

Run ID	Homogeneous medium strategy		Shell-Solid strategy	
[−]	δ_C [mm]	θ_C [°]	δ_C [mm]	θ_C [°]
3	−0.95	0.83	−0.97	0.68
4	−0.76	0.84	−0.97	0.77
7	−0.70	0.21	−0.77	0.15
8	−0.95	1.37	−1.12	1.04
10	−0.45	0.09	−0.88	0.22

on three indicators: printing time, total filament mass and mass of supports used during the 3D printing. The evaluation was carried out by using the ideaMaker® slicing software wherein the five optimized solutions are imported as STL files. As printing parameters, the standard RAISE3D Pro2® printing template was used, where the only modification was the suppression of the raft to obtain by difference the mass of the supports for each printing.

Fig. 15 shows the five printing preview of the G-code created after the slicing operations. It can be noted that the optimal solution obtained by imposing a drawing direction along the Y-axis (run ID 7) is characterized by topological features aligned with the building plate normal and, as a consequence, the resulting structure is essentially self-supporting with a very small quantities of supports required.

To identify those optimal solutions allowing for a trade-off between the printing time, the total filament mass and the mass of the supports to remove, the values of the printing time and of both the total filament mass and the fraction of filament mass used for the printing supports are shown in Fig. 16. Even though the optimal solution identified with the run ID 3 of Table 4 is characterized by the smallest volume fraction among those considered in this comparison (see Fig. 9(a)), the solution which minimizes both the printing time and the total mass is the one characterized by a drawing direction imposed along the Z-axis (see Fig. 8). Finally, as expected, the TO run where the drawing direction was defined along the Y-axis (see Fig. 8) is the one which requires the smaller quantity of supports.

8. Conclusions

In this paper, new hands-free door opener designs are proposed via TO and numerically assessed. Two sets of material parameters and optimization constraints of different nature (mechanical and

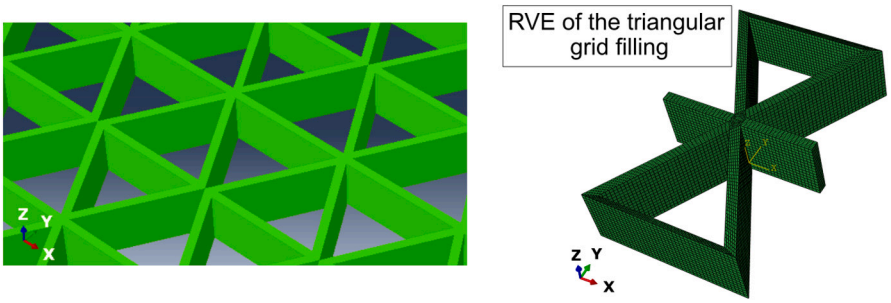

Fig. 13. On the right, FE model of the RVE of the triangular grid infill shown on the left.

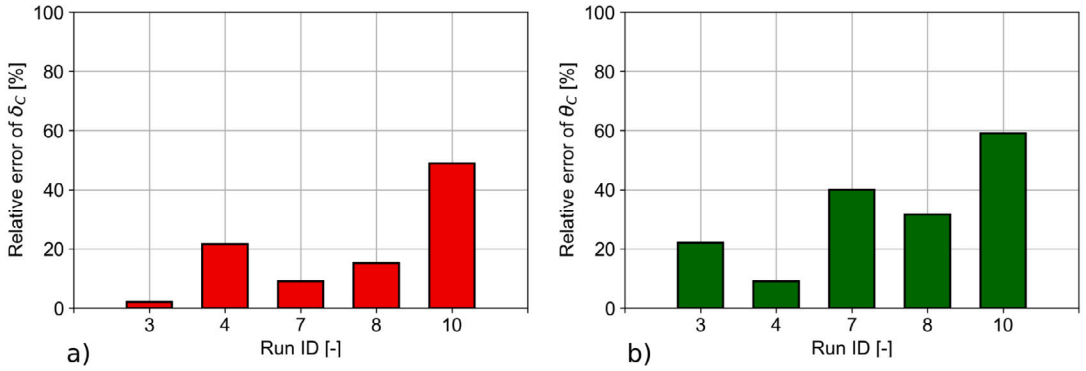

Fig. 14. Percentage values of the relative errors computed for the simulations of Table 7: in (a) the relative error of U_Z at point C and in (b) the relative error of θ_x at point C.

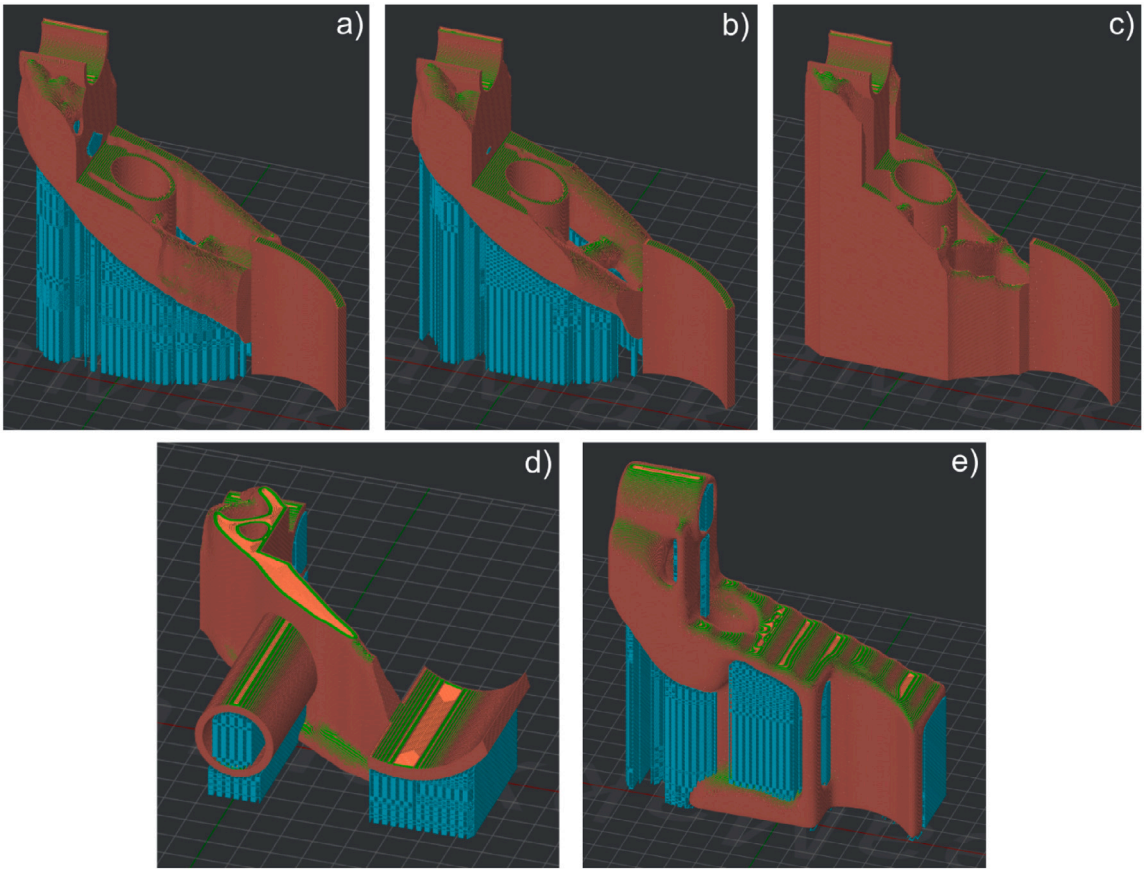

Fig. 15. Preview of the G-code files of the five optimal solutions obtained with the ELETI material: (a) run ID 3, (b) run ID 4, (c) run ID 7, (d) run ID 8 and (e) run ID 10. In red, the door opener optimal solutions to print and, in blue, the supports required by the printing process. (For interpretation of the references to color in this figure legend, the reader is referred to the web version of this article.)

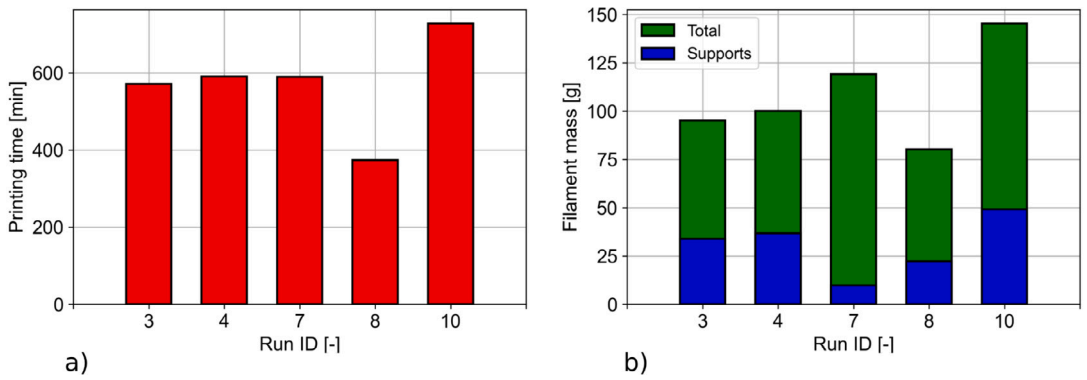

Fig. 16. In (a) the values of the printing time in minutes and in (b) the filament mass with the split between total mass and support mass for the optimized topologies of Fig. 15.

manufacturing-related requirements) have been considered. Moreover, a comparison between two topology optimization methods has been performed: the classic density-based method making use of the SIMP scheme and a recently developed method coupling NURBS entities with the SIMP approach.

Typical applications of 3D printing involve sandwich-like solutions where the external surface of the component is printed with a solid skin while the relative density and the repetitive geometry constituting the infill can be chosen according to the imposed requirements. In this context, two sets of equivalent material properties (isotropic and transversely isotropic) have been computed and applied in the FE models used for TO runs in order to evaluate their impact on the final topologies. Moreover, manufacturing constraints considering the minimum member size and the drawing direction have been included in the sensitivity campaign.

The results of the sensitivity campaign highlight that the influence of the two sets of material properties results in a local modification of the final topologies for both TO schemes. The imposed mechanical and manufacturing constraints are respected for all the optimal solutions and a more detailed mechanical assessment is performed via a shell-solid approach where the skin and the infill are modeled with suitable material properties. The comparison between the results of the models including equivalent material properties and those obtained with a more accurate material description shows that, according to the optimized topology under study, the relative error on the structural responses, i.e., vertical displacement and rotation of the point where external loads are applied, spans between 2% and 40%.

Moreover, optimized solutions are also evaluated with respect to indicators related to the 3D printing process such as the printing time, the total mass of filament used for the fabrication and the mass of supports required by the printing process. These indicators show that, among the considered optimal solutions, it is possible to find a trade-off between the total printing time, the total mass of used filament and the quantity of supports. Specifically, by imposing manufacturing constraints related to the drawing direction in the formulation of the optimization problem, it is possible to significantly reduce the quantity of supports during the printing process.

Declaration of competing interest

The authors declare that they have no known competing financial interests or personal relationships that could have appeared to influence the work reported in this paper.

Data availability

Data will be made available on request.

Acknowledgments

G. Bertolino is grateful to French National Research Agency for funding this study through the research project COFFA (Conception et Optimisation de Forme pour la Fabrication Additive) ANR-17-CE10-0008.

References

[1] B.H. Jared, M.A. Aguilo, L.L. Beghini, B.L. Boyce, B.W. Clark, A. Cook, B.J. Kaehr, J. Robbins, Additive manufacturing: Toward holistic design, Scr. Mater. 135 (2017) 141–147, http://dx.doi.org/10.1016/j.scriptamat.2017.02.029.
[2] B. Blakey-Milner, P. Gradl, G. Snedden, M. Brooks, J. Pitot, E. Lopez, M. Leary, F. Berto, A. du Plessis, Metal additive manufacturing in aerospace: A review, Mater. Des. 209 (2021) 110008, http://dx.doi.org/10.1016/j.matdes.2021.110008.
[3] C. Culmone, G. Smit, P. Breedveld, Additive manufacturing of medical instruments: A state-of-the-art review, Addit. Manuf. 27 (2019) 461–473, http://dx.doi.org/10.1016/j.addma.2019.03.015.
[4] A. García-Collado, J. Blanco, M.K. Gupta, R. Dorado-Vicente, Advances in polymers based multi-material additive-manufacturing techniques: State-of-art review on properties and applications, Addit. Manuf. 50 (2022) 102577, http://dx.doi.org/10.1016/j.addma.2021.102577.
[5] Y. Bozkurt, E. Karayel, 3D printing technology; methods, biomedical applications, future opportunities and trends, J. Mater. Res. Technol. 14 (2021) 1430–1450, http://dx.doi.org/10.1016/j.jmrt.2021.07.050.
[6] A. Bandyopadhyay, B. Heer, Additive manufacturing of multi-material structures, Mater. Sci. Eng. R 129 (2018) 1–16, http://dx.doi.org/10.1016/j.mser.2018.04.001.
[7] A. Prathyusha, G. Raghu Babu, A review on additive manufacturing and topology optimization process for weight reduction studies in various industrial applications, Mater. Today: Proc. 62 (2022) 109–117, http://dx.doi.org/10.1016/j.matpr.2022.02.604, International Conference on Advances in Materials and Mechanical Engineering.
[8] M. Bendsøe, N. Kikuchi, Generating optimal topologies in structural design using a homogenization method, Comput. Methods Appl. Mech. Engrg. 71 (2) (1988) 197–224.
[9] M. Bendsøe, O. Sigmund, Material interpolation schemes in topology optimization, Arch. Appl. Mech. 69 (1999) 635–654.
[10] M. Bendsøe, O. Sigmund, Topology Optimization - Theory, Methods and Applications, Springer, 2003.
[11] M. Bendsøe, Optimization of Structural Topology, Shape, and Material, Springer, 1995.
[12] M.B. e, E. Lund, N. Olhoff, O. Sigmund, Topology optimization - broadening the areas of application, Control Cybernet. 34 (2005) 7–35.
[13] J. Sethin, Level Set Methods and Fast Marching Methods - Evolving Interfaces in Com- Putational Geometry, Cambridge University Press, 1999.
[14] G. Allaire, F. Jouve, A. Toader, Structural optimization using sensitivity analysis and a level-set method, J. Comput. Phys. 194 (1) (2004) 363–393.
[15] M. Wang, X. Wang, D. Guo, A level set method for structural topology optimization, J. Comput. Phys. 192 (1) (2003) 227–246.
[16] M. de Ruiter, F. van Keulen, Topology optimization using a topology description function, Struct. Multidiscip. Optim. 26 (6) (2004) 406–416.
[17] Altair Engineering Inc, HyperWorks 13.0, OptiStruct user's guide, 2014.
[18] Simulia, tosca structure documentation 8.0, 2013.
[19] G. Costa, M. Montemurro, J. Pailhès, A 2D topology optimisation algorithm in NURBS framework with geometric constraints, Int. J. Mech. Mater. Des. 14 (4) (2018) 669–696.
[20] G. Costa, M. Montemurro, J. Pailhès, NURBS hyper-surfaces for 3D topology optimization problems, Mech. Adv. Mater. Struct. 28 (7) (2021) 665–684.

[21] G. Costa, M. Montemurro, J. Pailhès, Minimum length scale control in a NURBS-based SIMP method, Comput. Methods Appl. Mech. Engrg. 354 (2019) 963–989.
[22] T. Rodriguez, M. Montemurro, P. Le Texier, J. Pailhès, Structural displacement requirement in a topology optimization algorithm based on isogeometric entities, J. Optim. Theory Appl. 184 (2020) 250–276.
[23] M. Montemurro, G. Bertolino, T. Roine, A general multi-scale topology optimisation method for lightweight lattice structures obtained through additive manufacturing technology, Compos. Struct. 258 (2021) 113360, http://dx.doi.org/10.1016/j.compstruct.2020.113360.
[24] T. Roine, M. Montemurro, J. Pailhès, Stress-based topology optimisation through non-uniform rational basis spline hyper-surfaces, Mech. Adv. Mater. Struct. 29 (23) (2022) 3387–3407.
[25] M. Montemurro, K. Refai, A topology optimization method based on non-uniform rational basis spline hyper-surfaces for heat conduction problems, Symmetry 13 (5) (2021) 888, http://dx.doi.org/10.3390/sym13050888.
[26] M. Montemurro, On the structural stiffness maximisation of anisotropic continua under inhomogeneous Neumann–Dirichlet boundary conditions, Compos. Struct. 287 (2022) 115289, http://dx.doi.org/10.1016/j.compstruct.2022.115289.
[27] M. Montemurro, K. Refai, A. Catapano, Thermal design of graded architected cellular materials through a CAD-compatible topology optimisation method, Compos. Struct. 280 (2022) 114862, http://dx.doi.org/10.1016/j.compstruct.2021.114862.
[28] G. Bertolino, M. Montemurro, Two-scale topology optimisation of cellular materials under mixed boundary conditions, Int. J. Mech. Sci. 216 (2022) 106961, http://dx.doi.org/10.1016/j.ijmecsci.2021.106961.
[29] H.A. Colorado, D.E. Mendoza, H.-T. Lin, E. Gutierrez-Velasquez, Additive manufacturing against the Covid-19 pandemic: a technological model for the adaptability and networking, J. Mater. Res. Technol. 16 (2022) 1150–1164, http://dx.doi.org/10.1016/j.jmrt.2021.12.044.
[30] A. Kalkal, P. Allawadhi, P. Kumar, A. Sehgal, A. Verma, K. Pawar, R. Pradhan, B. Paital, G. Packirisamy, Sensing and 3D printing technologies in personalized healthcare for the management of health crises including the COVID-19 outbreak, Sensors Int. 3 (2022) 100180, http://dx.doi.org/10.1016/j.sintl.2022.100180.
[31] N. Vordos, D.A. Gkika, G. Maliaris, K.E. Tilkeridis, A. Antoniou, D.V. Bandekas, A. Ch. Mitropoulos, How 3D printing and social media tackles the PPE shortage during Covid – 19 pandemic, Saf. Sci. 130 (2020) 104870, http://dx.doi.org/10.1016/j.ssci.2020.104870.
[32] V. Maranha, P. Maia, L. Margalho, N. Lourenço, D. Oliveira, D. Maurício, J.F. Caseiro, L. Roseiro, Development of a dynamic hands-free door opener to prevent COVID-19 pandemic spreading, Designs 5 (3) (2021) 56, http://dx.doi.org/10.3390/designs5030056.
[33] P.-M. François, X. Bonnet, J. Kosior, J. Adam, R. Khonsari, 3D-printed contact-free devices designed and dispatched against the COVID-19 pandemic: The 3D COVID initiative, J. Stomatol. Oral Maxillo. Surg. 122 (4) (2021) 381–385.
[34] F. De Crescenzio, M. Fantini, E. Asllani, Generative design of 3D printed hands-free door handles for reduction of contagion risk in public buildings, Int. J. Interact. Des. Manufact. 16 (2022) 253–261.
[35] Y. Zhao, Y. Chen, Y. Zhou, Novel mechanical models of tensile strength and elastic property of FDM AM PLA materials: Experimental and theoretical analyses, Mater. Des. 181 (2019).
[36] M.-M. Pastor-Artigues, F. Roure-Fernández, X. Ayneto-Gubert, J. Bonada-Bo, E. Pérez-Guindal, I. Buj-Corral, Elastic asymmetry of PLA material in FDM-printed parts: Considerations concerning experimental characterisation for use in numerical simulations, Materials 13 (1) (2020).
[37] L. Gibson, M.F. Ashby, Cellular Solids Structure and Properties (Second Edition, Cambridge Solid State Science Series, 1997.
[38] O. Sigmund, J. Petersson, Numerical instabilities in topology optimization: A survey on procedures dealing with checkerboards, mesh-dependencies and local minima, Struct. Optim. 16 (1998) 68–75, http://dx.doi.org/10.1007/BF01214002.
[39] M. Montemurro, T. Roiné, J. Pailhès, Multi-scale design of multi-material lattice structures through a CAD-compatible topology optimisation algorithm, Eng. Struct. 273 (2022) 115009, http://dx.doi.org/10.1016/j.engstruct.2022.115009.
[40] L. Piegl, W. Tiller, The NURBS Book, Springer-Verlag, 1997.
[41] M. Montemurro, T. Rodriguez, P.L. Texier, J. Pailhès, Multi-displacement requirement in a topology optimization algorithm based on non-uniform rational basis spline hyper-surfaces, in: P.M. Mariano (Ed.), Variational Views in Mechanics, Springer International Publishing, Cham, 2021, pp. 223–257, http://dx.doi.org/10.1007/978-3-030-90051-9_9.
[42] G. Bertolino, M. Montemurro, N. Perry, F. Pourroy, An efficient hybrid optimisation strategy for surface reconstruction, Comput. Graph. Forum 40 (6) (2021) 215–241.
[43] J. Barbero, Finite Element Analysis of Composite Materials using Abaqus™, CRC Press, 2013.
[44] R. Luciano, E. Sacco, Variational methods for the homogenization of periodic media, Eur. J. Mech. A Solids 17 (1998) 599–617.